Journal of Materials Chemistry C

Accepted Manuscript

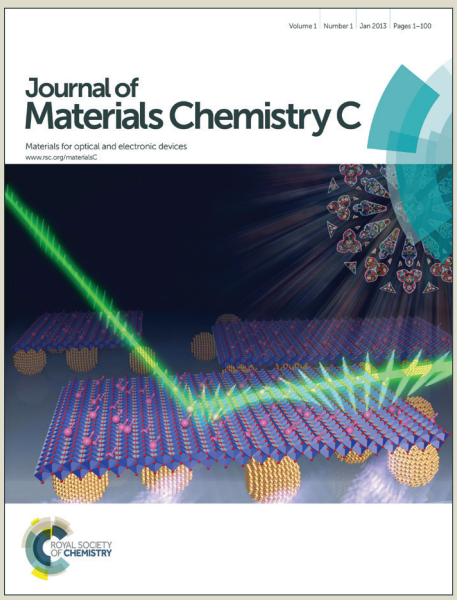

ROYAL SOCIETY OF CHEMISTRY

www.rsc.org/materialsC

Journal of Materials Chemistry C

PAPER

Block-assembling: A New Strategy of Fabricating Conductive Nanoporous Materials from Nanocomposites Based on a Melt-miscible Crystalline/Crystalline Blend and MWCNTs

Received 00th January 2015,
Accepted 00th January 2015

DOI: 10.1039/x0xx00000x

www.rsc.org/

Lijun Ye, Cuicui Ye, Xianchun Shi, Hongyan Zhao, Kangyuan Xie, Depei Chen, Yongjin Li*[a]

In this work, we are focusing on exploring a new way to prepare conductive nanoporous polymeric materials, by simply incorporating multi-walled carbon nanotubes (MWCNTs) into melt-miscible poly(L-lactic acid)/poly(oxymethylene) (PLLA/POM) blends. The POM components in the ternary nanocomposites crystallize first to form "nano-hybrid shish-kebab (NHSK)" structures at a high temperature in the presence of MWCNTs, with the simultaneous exclusion of poorly crystallizable PLLA chains into the intra-NHSK regimes. The subsequent PLLA crystallization in the intra-NHSK regimes is nucleated on the surface of MWCNTs as well to transform the final crystal morphology into "ternary-hybrid shish-kebab (THSK)" superstructures. Therefore, a "binary-polymer-decoration" of MWCNTs, named as "block-assembling", is achieved. Such a novel "block-assembling" structure is further used to fabricate conductive nanoporous polymeric materials with unique interposition structure of CNTs in the inner wall of the internal pores after removing of the PLLA components in the ternary nanocomposites.

Introduction

Due to their extraordinary properties, carbon nanotubes (CNTs) have attracted tremendous attention in past several decades.[1-4] Polymer-CNTs nanocomposites (PCNs) are considered as one of the first realized major commercial applications of CNTs.[1, 4-5] Incorporation of CNTs into polymers induces many attractive properties such as mechanical, electrical and thermal conductive, remotely actuated shape memory, electromagnetic interference shielding and sensing capability to the polymer matrix.[4] To facilitate the dispersion of CNTs, both chemical and non-covalent wrapping methods have been exploited to functionalize the surface of CNTs in many previous literatures.[6-14] Chemical functionalization by covalently linking functional groups to the CNTs surface will break the integral sp^2 conformation of the carbon atoms, resulting in the dramatic decrease of electrical and mechanical properties of the functionalized CNTs.[6, 12-14] The non-covalent methods using surfactants or polymers to wrap CNTs leads the interactions between CNTs and the wrapping molecules to be not as strong as the covalent bonding formed in the chemical methods.[6-7, 10] To blaze a trail, Li's group developed a unique strategy of applying semicrystalline polymers to functionalize CNTs via CNTs-induced polymer crystallization.[4, 15-16] Generally, CNTs are considered as 1-D nucleating agents (with numerous nucleating sites) that can accelerate crystallization of polymers.[4, 17-19] It has been realized that a small amount of CNTs can facilitate polymer crystallization while CNTs networks will impede the growth of crystals.

Li et al. first reported a "nano-hybrid shish-kebab (NHSK)" structure in polyethylene/CNTs (PE/CNTs) nanocomposites by solution crystallization under controllable conditions.[15] Moreover, Fu's group directly observed the formation of NHSK in bulk crystallization of high density polyethylene/CNTs (HDPE/CNTs) nanocomposites, via a dynamic packing injection molding technique (DPIM).[20-22] So far, many PCNs containing semicrystalline polymers, e.g., PE,[15-17, 20-21, 23-36] polyamide (PA),[15-17, 19, 37-40] isotactic polypropylene (*i*-PP),[22, 36] poly(lactic acid) (PLLA),[18, 22, 41-43] polyoxymethylene (POM),[44] poly(ethylene oxide) (PEO),[42, 45] poly(vinyl alcohol) (PVA),[45-46] poly(butylene terephthalate) (PBT),[47] poly(vinylidene fluoride) (PVDF),[37, 45] polytetrafluoroethylene (PTFE),[48-49] polyacrylonitrile (PAN),[45, 50] poly(3-hexylthiophene) (P3HT),[51] PE-*b*-PEO,[52] PE-*b*-SBR [53] and poly(vinylcyclohexane)-*b*-(ethylene)-*b*-(vinylcyclohexane) (PVCH–PE–PVCH) [54] have been reported to observe the formation of NHSK. The NHSK where the CNTs inside are regarded as the "shish", while the periodically decorating polymer lamellae in a "disk-shape" are perpendicular to the CNT axis to be the "kebabs". The formation mechanism of NHSK is generally considered to be "size-dependent soft epitaxy (SSE)", as proposed by Li et al.[16]

The melt-miscible crystalline/crystalline blends exhibit varieties of phase morphologies and superstructures depending on blending compositions and crystallization conditions.[55-56] At a given crystallization temperature (T_c), the high-T_c component crystallizes while low-T_c one still remains amorphous and acts as a diluent. The low-T_c component might locate in the interlamellar, interfibrillar or interspherulitic regimes of the pre-existed framework of the high-T_c

[a] College of Materials, Chemistry and Chemical Engineering, Hangzhou Normal University, Hangzhou 310036, People's Republic of China.
E-mail: Yongjin-li@hznu.edu.cn

† Electronic Supplementary Information (ESI) available. Tables. S1-S2, Video. S1, Figs. S1-S8. See DOI: 10.1039/ x0xx00000x

one.[57-60] Varieties of works focused on the morphology and crystallization behaviors of melt-miscible crystalline/crystalline blends have been delicately reviewed by Jungnickel [56] and Schultz.[61-62] PLLA/POM blends are melt-miscible crystalline/crystalline systems. According to our previous work, PLLA/POM blends exhibit the typical lower critical solution temperature (LCST) phase behavior at above the melting temperature of POM.[63] Moreover, we have systematically investigated the crystallization behaviors of PLLA/POM blends. A small amount of POM fragment crystals in PLLA/POM blends serve as PNAs, leading to the enhancement of PLLA crystallization, while a large quantity of POM strongly hinders the crystallization of PLLA due to the formation of compact spherulites.[64] In our recent work, the poorly crystallizable PLLA molecular chains are found to be excluded into the interlamellar and/or interfibrillar regimes of POM crystals during the POM crystallization and the subsequent PLLA crystallization is extensively confined in the POM banded-spherulitic frameworks.[65] Such an interlamellar and/or interfibrillar inclusion of PLLA in the POM frames is further exploited to make nanoporous polymeric materials with hierarchical patterned surface and 3-D interpenetrated internal channels by removal of the PLLA components in the binary blends. And the tuning of hierarchical patterned structure and the size of internal channels can be easily realized by adjusting the crystallization conditions.

In this work, MWCNTs are incorporated into PLLA/POM blends with a focus on exploring a new and simple path to fabricate conductive nanoporous polymeric materials. The crystallization behaviors of the PLLA/POM/MWCNTs nanocomposites have been investigated. It is found that POM component first crystallizes onto the surface of MWCNTs to form the NHSK superstructures at a high temperature, with the simultaneous expulsion of the poorly crystallizable PLLA chains into the intra-NHSK regimes (the spacing between the adjacent kebab crystals of POM along a nanotube). Due to the relatively high MWCNTs content for POM crystallization, only parts of nanotubes are covered by POM kebab crystals. Upon being further cooled to T_c of PLLA, the PLLA molecular chains are nucleated by MWCNTs as well to translate the final crystal morphology of the ternary nanocomposites into "ternary-hybrid shish-kebabs (THSK)" structure, in which POM and PLLA sequentially decorate onto a same nanotube to share the "shish" in common and two types of crystals grow to be the "binary-hybrid kebabs". Therefore, a novel "binary-polymer-decoration" structure of MWCNTs, named as "block-assembling", is achieved. Such a novel "block-assembling" structure is further used as a new, simple and feasible template to make conductive nanoporous polymeric materials by a selective solvent etching of PLLA components in the ternary nanocomposites.

Experimental

Materials and Sample Preparation

The PLLA (3001 D) materials contained 1.6 % of D-lactide were purchased from Nature Works Co. LLC, USA. The M_n and M_w/M_n were 89300 ± 1000 g mol^{-1} and 1.77 ± 0.02, respectively. The POM (MC 90) samples are kindly provided by Shenhua Co., Ltd., China. The melt flow index is 9.23 g 10 min^{-1}. The M_w and M_w/M_n of the POM sample are 174300 g mol^{-1} and 2.19, respectively. MWCNTs were provided by Showa Denko K. K., Japan.

All samples have been dried in an 80 ^{o}C vacuum oven for 12 h beforehand. And then, PLLA, POM and MWCNTs were blended at 190 ^{o}C using a batch mixer (Haake Polylab QC) with a twin screw at an initial rotation speed of 20 rpm for 1 min and subsequently raised to 50 rpm for 5 min. All the samples prepared were firstly hot-pressed at 190 ^{o}C under a pressure of 14 MPa for 3 min to thin films with a thickness of 300 μm, followed by a rapid cooling process to room temperature.

Extractions were performed in a Soxhlet extraction apparatus. The PLLA components are extracted with chloroform and, therefore, can as well be referred to as the porogen phase. The temperature of the chloroform in the Soxhlet extraction apparatus was about 60 ^{o}C. Following the extractions, the samples were dried in a 40 ^{o}C vacuum oven.

Sample Characterizations

The crystallization behaviors of the prepared samples were measured in a differential scanning calorimeter (DSC Q 2000) under nitrogen flow at a heating rate of 10 ^{o}C min^{-1} from 10 ^{o}C to 200 ^{o}C, held for 5 min to erase the thermal history before being further cooled down to 10 ^{o}C in a cooling rate of 10 ^{o}C min^{-1}. The heating and cooling DSC traces were recorded. The heat flow and temperature of the instrument were calibrated with sapphires and pure indium, respectively, before sample scanning.

Morphology of the samples of the obtained ternary nanocomposites was observed by field-emission scanning electron microscope (FESEM). A Hitachi S-4800 SEM system was used for SEM measurements at an accelerating voltage of 1 and 3 kV. All the samples were fractured after immersion in liquid nitrogen for about 15 min. The structure of the samples was also observed using a transmission electron microscope (TEM) (Hitachi HT 7700) operating at an acceleration voltage of 100 kV. The blend samples were ultramicrotomed at -120 ^{o}C to a section with a thickness of about 80 nm. The sections are then stained by ruthenium tetroxide (RuO_4) for 4 h.

Infrared spectra of samples were recorded on a Nicolet 6700 time-resolved Fourier transform infrared spectrophotometer (FTIR). The samples were sandwiched between a pair of KBr plates. Thermal treatments were performed in a temperature cell accessory controlled with an Omega Temperature Controller within an accuracy of ± 1 ^{o}C. The samples were firstly heated to 190 ^{o}C in a 10 ^{o}C min^{-1} rate, held for 10 min to completely erase the thermal history, and then rapidly cooled to 135 ^{o}C for isothermal crystallization. IR spectra of the specimens are then collected in an interval of 30 s. Nitrogen adsorption-desorption isotherms were measured by a Quantachrome Autosorb 6B sorption analyzer. The pore-size distribution was derived from the adsorption branch of the isotherms by the Barrett-Joyner-Halenda (BJH) method. The resistivity of the samples was measured according to the testing method for resistivity of conductive plastics with four-point probe array (JIS K7194).

Results

Finely Dispersed MWCNTs and the Effects of MWCNTs on the Miscibility of PLLA and POM.

A small amount of MWCNTs are blended with PLLA and POM to fabricate the ternary nanocomposites with the indicated compositions. Fig. 1 shows the typical SEM image of the ternary nanocomposites and the composition of the sample in Fig. 1 is 50/50/0.5. Without any distinct agglomerates, MWCNTs are successfully incorporated into PLLA/POM blends, as shown in Fig. 1, indicating the fine dispersion of nanotubes into the matrix of PLLA and POM. And the modulus, yield strength and breaking strength of PLLA/POM blends have been significantly enhanced with the addition of MWCNTs (Fig. S1). However, two distinct glass transition temperatures (T_g) are observed for the PLLA/POM/MWCNTs samples quenched from the melt state (Fig. S2), indicating that PLLA and POM are phase-separated during the quenching process. Even in PLLA/POM blends without MWCNTs, as previously exhibited, the phase separation of PLLA and POM are observed when cooling down from melt miscible region.[63] It appears very different from the well-defined PVDF/PBA blends with the typical LCST phase Behaviors, exhibiting two distinct melting temperatures (T_m) but only a single T_g over the entire composition range.[66-69] Actually, we have found that the PLLA/POM blends exhibit both the LCST and UCST-type phase Behaviors in our very recent work (Fig. S3) and the details will be discussed in a near future report. Moreover, the POM components in the ternary nanocomposites crystallize into the NHSK superstructures between the LCST and UCST in this work. In other words, there has been no phase separation occurring before and after the crystallization of POM.

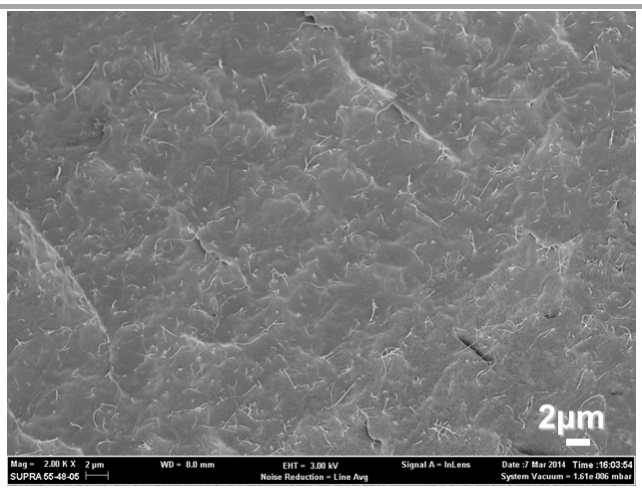

Fig. 1 The typical SEM image of the ternary nanocomposites (the sample is the PLLA/POM/MWCNTs (50/50/0.5) composite).

Morphology and Crystallization Behaviors of PLLA/POM/MWCNTs Ternary Nanocomposites

The DSC cooling curves of neat PLLA, POM, PLLA/POM and PLLA/POM/MWCNTs samples with the indicated compositions are shown in Fig. 2. Although both PLLA and POM are crystallizable polymers, the former has a much lower crystallization rate than the latter one. It can be clearly seen in Fig. 2 that no exothermic peaks for the PLLA crystallization are observed for all samples when cooled in a 10 °C/min rate from the melts (as confirmed by the WAXD patterns in Fig. S4, where no diffraction for PLLA crystals has been observed). With the incorporation of PLLA, moreover, a shift of T_c to a lower one manifests itself the crystallization rate of POM in the PLLA/POM blends has been distinctly restrained for the blends without MWCNTs. Upon the addition of MWCNTs (from 0.1 wt % to 1.0 wt %), the crystallization rate of POM in the PLLA/POM/MWCNTs nanocomposites increases drastically, implying that the crystallization of POM is efficiently accelerated by MWCNTs. Fig. 3 shows the typical TEM image of the ternary nanocomposites and the composition of the sample exhibited in Fig. 3 is 50/50/1.0. It is clear to see from Fig. 3 that the typical NHSK superstructure (POM crystal-decorated MWCNTs) is distinctly observed in the ternary nanocomposites. Although the MWCNT cannot be so clearly identified due to the coverage of polymers in these images, the consistent orientations of the adjacent lamellae and the aspect ratios of the novel "lamellar-orientation areas" indicate that the axis of the underlying nanotube is perpendicular to the POM lamellae.

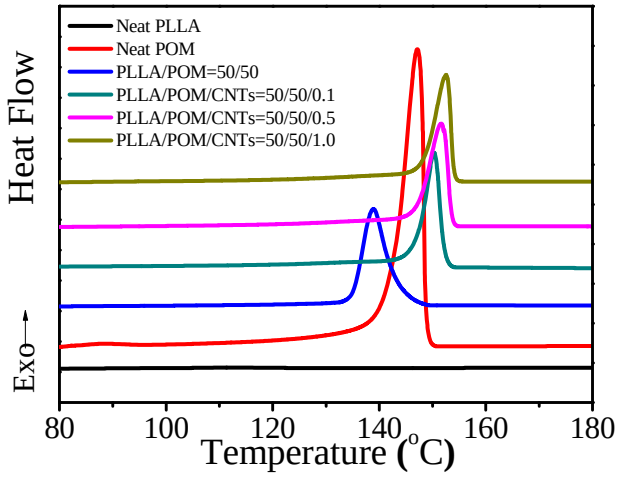

Fig. 2 The DSC curves of Neat PLLA, PLLA/POM, PLLA/POM/MWCNTs samples quenched from the melt state in a 10 °C/min cooling rate.

Interestingly, the crystallinity of POM in the ternary nanocomposites keeps almost constant, as shown in Table. S1, with the addition of MWCNTs. On the one hand, without considering the dimensional changes of kebab crystals, as we supposed, the mean number of POM kebabs decorating onto a single nanotube might decrease upon the increasing loading of MWCNTs, leading the spacing between the adjacent kebab crystals (the intra-NHSK regimes) to be extended. One the other hand, as reported in PE/SWCNTs systems by Li et al, the PE kebab crystal size increases upon the decreasing of SWCNTs contents.[33] It comes to conclude that the coverage rate of nanotubes will probably decrease with the increasing amount of MWCNTs, leading to the enlargement of spacing between the adjacent kebab crystals.

To make a detail understanding of the crystallization behaviors, the crystallization behaviors of PLLA/POM/MWCNTs nanocomposites with 1.0 wt % loading of MWCNTs and the PLLA/POM compositions varying from 100/0 to 0/100 have been systematically investigated, as shown in Fig. 4. It can be seen from Fig. 4 that two exothermic peaks for the crystallization of PLLA and POM are distinctly observed in the ternary nanocomposites in which PLLA acts as a major component (as convinced by Fig. S5),

when being cooled in a 10 °C/min rate from the melt state. The crystallization of PLLA has been dramatically accelerated while the T_c of POM is slightly altered. In this case, POM molecular chains crystallize first onto the surface of MWCNTs and form the NHSK superstructures at a high temperature, as we speculated, leading to the expelling of the poorly crystallizable PLLA chains into the intra-NHSK regimes. Therefore, the subsequent PLLA crystallization in the intra-NHSK regions might be controlled by two possible factors. On the one hand, the initial nucleation of PLLA molecular chains are mainly controlled by the quantity of nucleating sites remained on the "bare" surface (unoccupied by POM crystals) of MWCNTs after POM crystallization. On the other hand, the further growth of PLLA crystals is very dependent on the spacing between the adjacent kebab POM crystals.

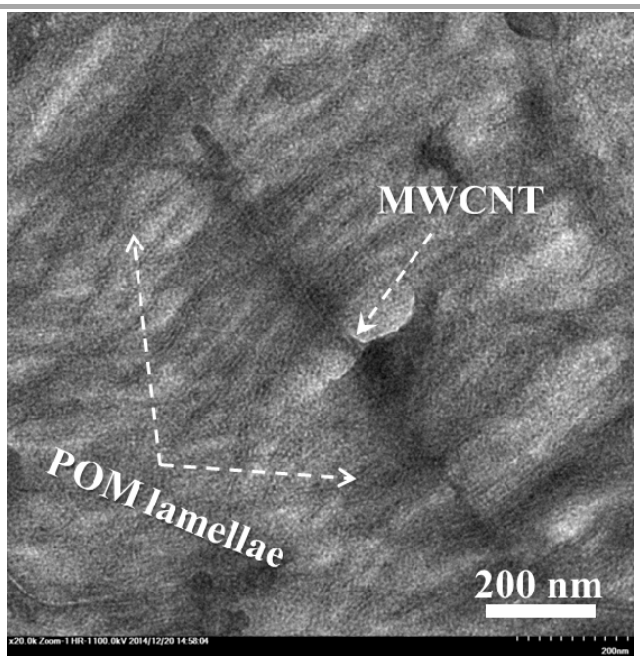

Fig. 3 The typical TEM image of the ternary nanocomposites (the sample is the PLLA/POM/MWCNTs (50/50/1.0) composite).

Moreover, with the increasing concentration of PLLA, the crystallization rate and crystallinity of PLLA are significantly enhanced (Table. S2). It might be ascribed to the increasing amount of nucleating sites left in the intra-NHSK regimes and the extending of the spacing between the adjacent kebab POM crystals, due to the decreasing of POM concentration (that is, the increasing of the relative MWCNTs/POM compositional ratios in the ternary nanocomposites leads to the decreasing coverage rate of nanotubes). After the subsequent PLLA crystallization, the crystal morphology is translated into the THSK superstructures, in which POM and PLLA are sequentially nucleated by MWCNTs to share the "shish", and further, grow to be the "binary-hybrid kebabs", leading to a "block-assembling" decoration of two polymers crystals on MWCNTs. Such a "binary-hybrid-kebab" decoration of CNTs (shish), with the novel THSK structure, in the ternary nanocomposites has been seldom reported before.

However, no exothermic peaks for the PLLA crystallization can be seen in the ternary nanocomposites with the PLLA loading less than 60 wt %. On the one hand, it might be originated from the increasing surficial occupation rate of MWCNTs by the first crystallized POM crystals, leading to the shrinking of the intra-NHSK regimes along a nanotube and a small amount of nucleating sites remained for nucleating the PLLA included in the intra-NHSK regions to crystallize. On the other hand, the growth of PLLA crystals might be confined in the pre-formed solid frameworks, when the POM components are in high concentrations. The "bare" surface of MWCNTs, as we considered, will certainly deceases with the increasing concentration of POM to reach a higher surficial coverage of nanotubes, and meanwhile, the spacing of the intra-NHSK regimes will definitely being narrowed. Therefore, the confinement of the PLLA crystallization mentioned above will become increasingly apparent with the further increasing content of POM. In this case, a "block-assembling" decoration structure of POM crystals and amorphous PLLA chains on MWCNTs generates eventually.

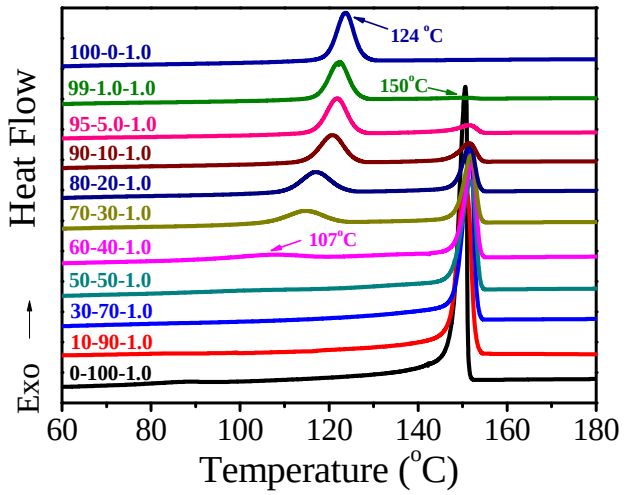

Fig. 4 The DSC curves of PLLA/POM/MWCNTs samples with the indicated compositions quenched from the melt state in a 10 °C/min cooling rate.

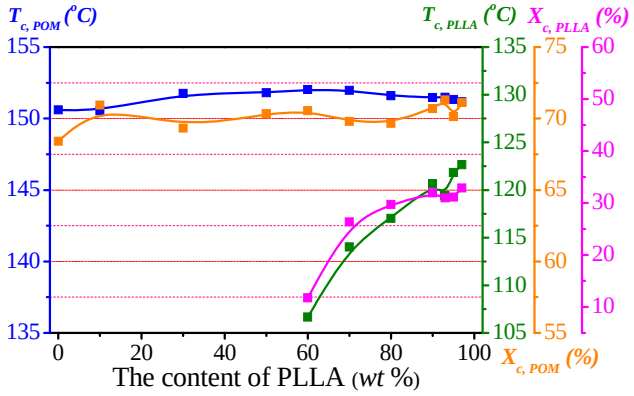

Fig. 5 The PLLA compositional effects on the crystallization of PLLA and POM in the ternary nanocomposites with 1.0 wt % loading of MWCNTs.

Fig. 5 shows the PLLA compositional effects on the crystallization of PLLA and POM in the ternary nanocomposites. It is clear seen from Fig. 5 that both the crystallization rate and crystallinity of PLLA are obviously enhanced with the increasing amount of PLLA (Table. S2). Interestingly, the crystallization rate and crystallinity of POM in the ternary nanocomposites changes slightly upon the varying of PLLA content. It might be attributed to the "saturation" of MWCNTs for nucleating the POM crystallization. The "saturation" here means that the loading of MWCNTs is adequate for the POM crystallization in the ternary nanocomposites, and further, no completely but partially covered nanotubes are left

after the crystallizing of POM, so as the subsequent PLLA crystallization to be probably nucleated on the "bare" surface of MWCNTs in the intra-NHSK regimes, with the translating of the final crystal morphology into the THSK superstructures (that is, the "block-assembling" decoration structure of two polymer crystals on MWCNTs).

The Intra-NHSK Inclusion of PLLA in the PLLA/POM/MWCNTs ternary nanocomposites

The nucleation effects of MWCNTs on POM in the ternary nanocomposites have been clearly demonstrated. In order to fully understand the following PLLA crystallization behaviors in presence of both MWCNTs and POM crystals, time-resolved FTIR measurements have been carried out to trace the crystallization of PLLA in the ternary nanocomposites. Fig. 6 shows the representative time-resolved FTIR spectra of the PLLA/POM/MWCNTs (70/30/1.0) nanocomposite during isothermal crystallization of PLLA at 135 ^{o}C. Note that, in this case, POM component has already crystallized during the quenching process to 135 ^{o}C for the PLLA isothermal crystallization. The bands at 921, 1210, and 1456 cm^{-1} are generally corresponded to intra-chain 10_3 helix formation, the combination of –COC- and -CH_3 inter-chain interaction and -CH_3 inter-chain interaction of PLLA, respectively. However, the band at 921 cm^{-1} that recognized as being related to crystallization has not been clearly observed due to the overlapping with the vibrations of POM chains. But quite noticeably, the 866 cm^{-1} band shifts to 872 cm^{-1} simultaneously with the increasing of the crystallization time, as shown in Fig. 6(b), indicating a transition of the PLLA molecular chains to a well-defined order (the crystalline state). It is found from Fig. 6(a) that the 1210 cm^{-1} band exhibits a faster and more sensitive response to inter-chain conformational ordering than the 1456 cm^{-1} one. The band at 1210 cm^{-1} is assigned to an E1 mode (perpendicular to the helix axis) and its intensity increases because the transition moments corresponding to the conformers change their orientation from a random arrangement to an *in-plane* orientation.[70] According to the previous work reported by Li et al, the intensity increase is originated from the unique template effect of CNTs on the conformational ordering of PLLA.[18, 71] During the crystallizing process, PLLA molecular chains adsorbed the MWCNTs via the CH-π interaction and subsequent PLLA backbones contacted with the pre-adsorbed ones through (–COC- + -CH_3) interactions to form a unique conformational ordering structure, which finally became the precursor for crystal growth.

The results above give us direct evidence that the PLLA is nucleated by MWCNTs as well. In other words, the PLLA molecular chains are simultaneously excluded into the intra-NHSK regimes during the crystallization of POM. The same conclusions can be easily drawn from the time-resolved FTIR spectra of the PLLA/POM/MWCNs (90/10/1.0) nanocomposites (Fig. S6). In a word, both POM and PLLA nucleate on the surface of MWCNTs, resulting in a novel "block-assembling" decoration of two polymers crystals on nanotubes in PLLA/POM/MWCNTs ternary nanocomposites (as confirmed by the 2D WARD measurement in Fig. S7, which implies the PLLA molecular chains are parallel to the POM ones as well as the axes of MWCNTs). Such a "block-assembling" decoration of two polymers (crystals and/or molecular chains) on CNTs gives a new promise of fabricating conductive nanoporous polymeric materials by selective removal of the PLLA components in the ternary nanocomposites.

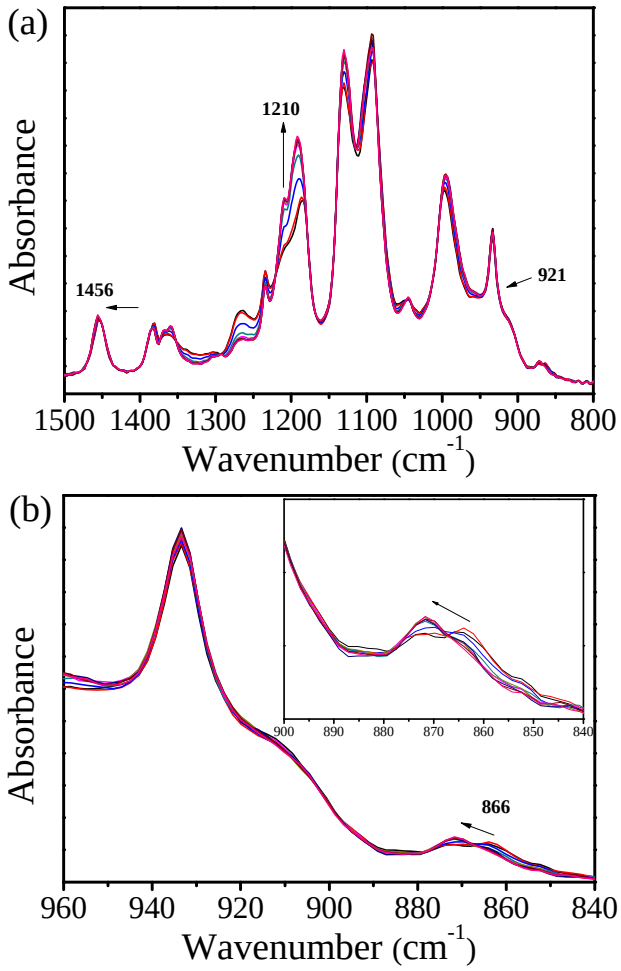

Fig. 6 The time-resolved FTIR spectra of the PLLA/POM/MWCNTs (70/30/1.0) nanocomposite during isothermal crystallization of PLLA at 135 ^{o}C (0-480 s).

Conductive Nanoporous Polymeric Materials Obtained from Nanocomposites of PLLA/POM/MWCNTs after the Extraction of PLLA.

The ternary nanocomposites are further made into thin films and carried out solvent etching by chloroform (Soxhlet extraction). Fig. 7(a) shows the macroscopic image of PLLA/POM/MWCNTs (50/50/0.5) nanocomposite film after solvent etching by chloroform (Soxhlet extraction). It can be clearly seen that the extracted film not only maintains the original shape, but is also flexible. It is, moreover, calculated by a gravimetric method that almost all the PLLA is extracted (close to 100 %) and the extracted solution always keeps colourless and transparent, implying that majority of MWCNTs are still contained in the residue materials (Fig. S8). It is further to find that water can continuously flow through the thin films after the extracting of the PLLA component (Video. S1), indicating the interpenetrated internal pore structure nature. These results indicate that the NHSKs of POM crystals are not separated but connected with each other to serve as a sturdy framework for the final porous materials. The PLLA component included in intra-NHSK regimes forms a highly-continuous phase during the expelling

out from the initial homogeneous melts, so as to be mostly etched to endow the residue materials with internal channels.

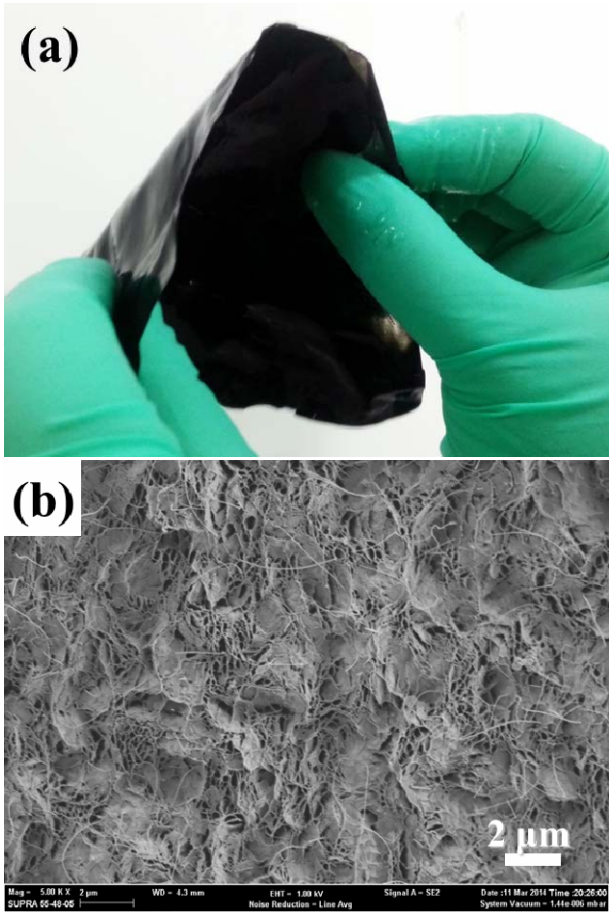

Fig. 7 (a) The macroscopic image and (b) the typical SEM images of the fracture surface of the PLLA/POM/MWCNTs (50/50/0.5) nanocomposite after solvent etching.

Fig. 7(b) shows the typical SEM image of the fracture surface of the PLLA/POM/MWCNTs (50/50/0.5) nanocomposite after the extraction of PLLA. Numerous narrow channels are found to disperse in the internal of the residue material after etching. It is obvious that all the narrow channels are generated by the solvent etching process of PLLA that initially located in the intra-NHSK regimes. Fig. 8(a) shows the N_2 adsorption-desorption isotherm of the PLLA/POM/MWCNTs (50/50/0.5) nanocomposite after solvent etching of PLLA. The isotherm of the sample obtained from the 50/50/0.5 nanocomposite is typically of type IV with a capillary condensation step and the capillary condensation step in the isotherm is very sharp, indicating the slit (typical lamellar stacking) and mesoporous nature of the pore structure. The BJH method takes into account the capillary condensation using the Kelvin equation and it is useful for the determination of the pore-size distribution generally for meso-pores.[72] Fig. 8(b) shows the pore-size distributions of the sample obtain from the 50/50/0.5 nanocomposite. Note that, the structure of the slit pores in the obtained sample is anisotropy (as convinced by the SEM image) and the pore size measured here is much closer to the narrow width of the pores.

It can be further found from Fig. 7(b) that MWCNTs are still contained and finely dispersed in the final porous material. The conductivities of the ternary nanocomposites before and after solvent etching are respectively measured as well, as shown in Table. 1. It is clear from Table. 1 that the conductivities of the PLLA/POM/MWCNTs nanocomposites after etching dramatically increase with the addition of MWCNTs (from 0.1 wt % to 1.0 wt %). Moreover, the conductivity of PLLA/POM/MWCNTs (50/50/0.5) nanocomposite remarkably increases from 10^{-7} S/cm to 10^{-3} S/cm after etching, again indicating that MWCNTs are not only covered with POM but PLLA instead of being packed only by POM crystals in the ternary nanocomposites.

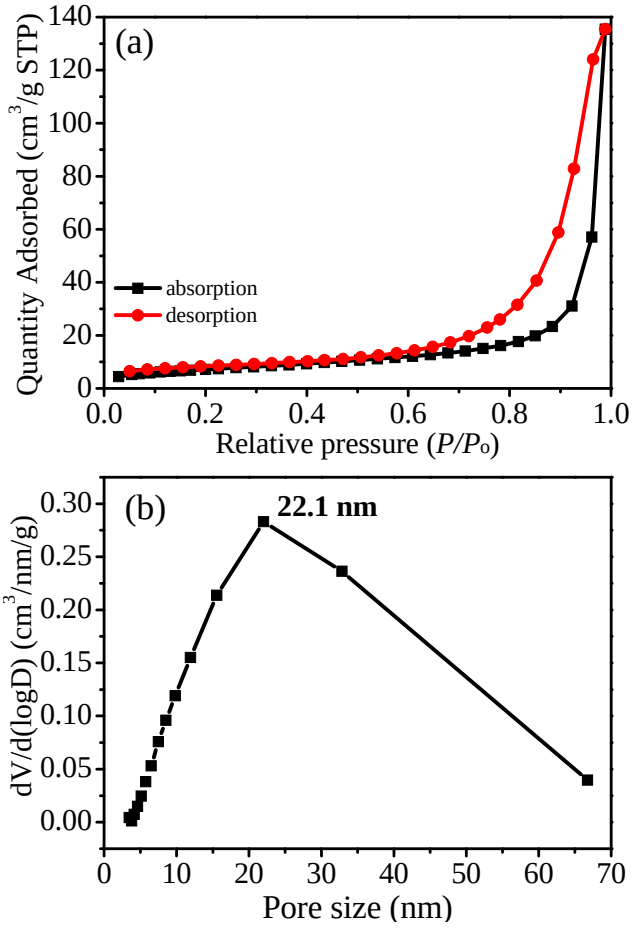

Fig. 8 (a) N_2 adsorption-desorption isotherm (b) Pore size distributions of the PLLA/POM/MWCNTs (50/50/0.5) nanocomposite after solvent etching.

If all the MWCNTs are packed by POM chains (that's, phase separation occurs in the melt state and nanotubes are to be embedded in the POM phase), as we considered, the remarkable changes of the conductivity would not have happened due to the same relative content of MWCNTs contained in the matrixes (where MWCNTs are actually located), before and after etching. Most interestingly, the surface of MWCNTs initially covered by PLLA component (crystals or molecular chains) is to be exposed, with the forming of the interposition structure of nanotubes in the inner wall of the internal channels after solvent etching of PLLA components in the ternary nanocomposites. Such a novel pore structure will certainly and significantly improve the conductivity of the final porous materials. We can, therefore, conclude that the intra-NHSK inclusion of PLLA in the PLLA/POM/MWCNTs nanocomposites gives

us a new, simple and feasible strategy to fabricate conductive nanoporous polymeric materials.

Table 1 The electrical conductivity of PLLA/POM/MWCNTs nanocomposites with the indicated compositions, before and after etching

Sample Name	Surface Resistivity (Ω/□)	Volume Resistivity (Ω·cm)	Conductivity (S/cm)	
			Before Etching	After Etching
50/50/0.1	--	--	--	--
50/50/0.5	5.629×10^{7}	2.585×10^{6}	4.501×10^{-7}	8.006×10^{-3}
50/50/1.0	2.729×10^{3}	1.255×10^{2}	9.325×10^{-3}	1.432×10^{-2}

Discussion

From the above, we have successfully explored a novel "block-assembling" strategy to fabricate conductive nanoporous polymeric materials from nanocomposites based on a melt-miscible PLLA/POM blend and MWCNTs. With the incorporation of MWCNTs, the POM components in the ternary nanocomposites crystallize first onto the surface of MWCNTs to form the NHSK superstructures in the presence of amorphous PLLA chains, resulting in the partial but not complete coverage of MWCNTs. During the crystallizing of POM, the PLLA molecular chains are proved to be excluded into the intra-NHSK regimes of POM crystal, as illustrated in Scheme. 1. When the POM acts as major components, the PLLA molecular chains included in the intra-NHSK regions are still in amorphous state after being further cooled to the room temperature (following the crystallization of POM), as shown in Scheme. 1(a), leading to a "block-assembling" decoration structure of POM crystals and amorphous PLLA chains on the surface of MWCNTs. With the decreasing content of POM, the subsequent PLLA crystallization in the intra-NHSK regions is nucleated by MWCNTs as well and the PLLA lamellae come out of the "bare" surface of nanotubes to translate the final crystal morphology into the THSK superstructures, as shown in Scheme. 1(b), resulting in the "block-assembling" decoration structures of two polymer crystals on MWCNTs. On the one hand, it might be ascribed to the numerous nucleating sites left on the "bare" surface of MWCNTs in the intra-NHSK regimes due to the decreasing coverage rate of nanotubes. On the other hand, the spacing between the adjacent kebab POM crystals are extended with the decreasing of POM, so as the PLLA lamellae coming out of the "bare" surface of MWCNTs (the intra-NHSK regions) to be well-developed.

After selective solvent removing of the PLLA component included in the intra-NHSK regimes, conductive nanoporous polymeric materials with unique interposition structure of CNTs in the inner wall of the internal pores can be easily achieved, as illustrated in Scheme. 1. Such a novel "block-assembling" decoration of two polymers (crystals and/or molecular chains) on MWCNTs gives us a new, simple and feasible path to fabricate conductive porous polymeric materials from the ternary nanocomposites based on a melt-miscible blend and MWCNTs. Moreover, the pore size, surface areas and conductivity of the obtained nanoporous polymeric materials can be further expected to be modulated by varying the compositions and crystallization conditions. The detail manipulation of pore structure and conductivity is under investigation and will be reported in the near future.

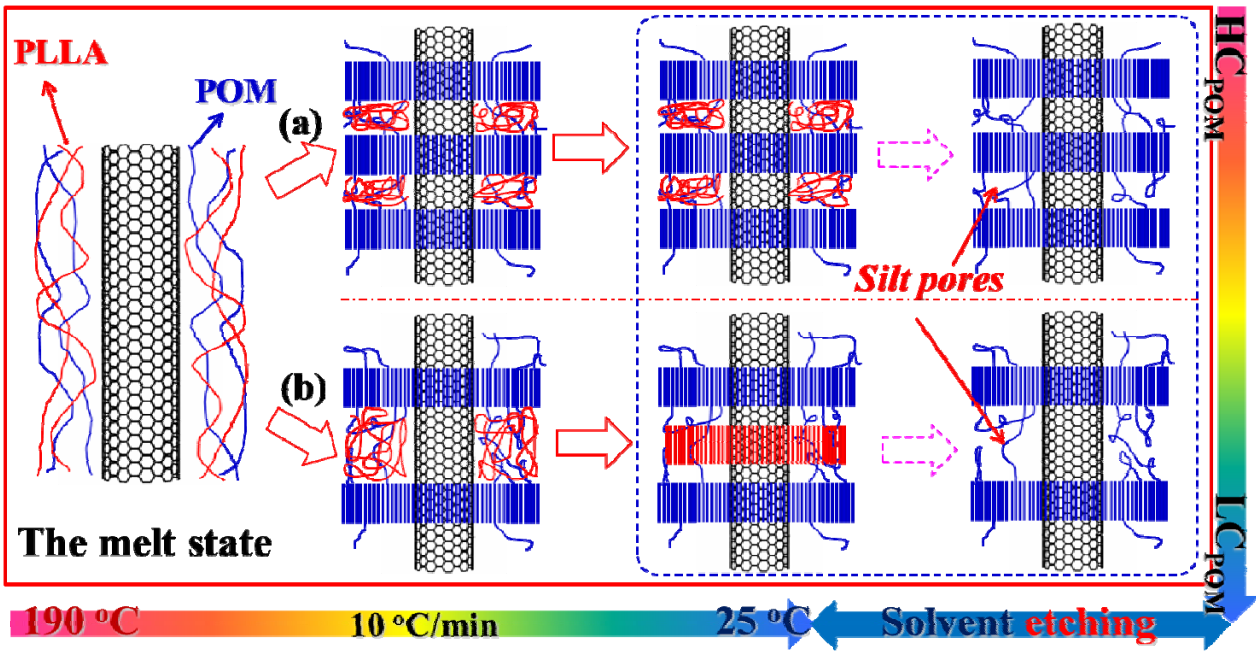

Scheme. 1 The schematic illustration of fabricating conductive nanoporous polymeric materials via the "block-assembling" strategy based on PLLA/POM/MWCNTs ternary nanocomposites.

Conclusions

A "block-assembling" decoration of two polymers on nanotubes in a nanocomposite comprised of melt-miscible PLLA/POM blends and MWCNTs has been exploited to prepare conductive nanoporous polymeric materials. The POM molecular chains in the ternary nanocomposites are nucleated by MWCNTs and crystallize first into the NHSK superstructures at a high temperature, leading to the simultaneous expulsion of PLLA chains into the intra-NHSK regimes of POM crystals and the "block-assembling" decoration structure of two polymers on MWCNTs. Moreover, the PLLA chains included in the intra-NHSK spacing are also nucleated by MWCNTs to translate the crystal morphology into the THSK superstructures (that is, a novel "block-assembling" decoration structure of two polymer crystals on the surface of MWCNTs), when the PLLA acts as a major component. After selective removal of the PLLA components in the intra-NHSK regimes of the ternary nanocomposites, conductive nanoporous polymeric materials can be easily achieved. Furthermore, it is expected that the tuning of pore size, surface areas and conductivity of the conductive nanoporous polymeric materials can be realized by adjusting compositions and crystallization conditions.

Acknowledgements

This work was financially supported by the National Science Foundation of China (51173036, 21374027) and the Ministry of Education Program for New Century Excellent Talents (NCET-13-0762).

Notes and references

‡ College of Materials, Chemistry and Chemical Engineering, Hangzhou Normal University, Hangzhou, 310036, P. R. China. FAX: +86 571 28867899; Telephone: +86 571 28867026; E-mail: Yongjin-li@hznu.edu.cn.
† Electronic Supplementary Information (ESI) available: Tables. S1-S2, Video.S1, Figs. S1-S8. See DOI: 10.1039/b000000x/.

1. R. H. Baughman, A. A. Zakhidov, W. A. de Heer, *Science*, 2002, **297**, 787.
2. M. Terrones, *Annu. Rev. Mater. Res.*, 2003, **33**, 419.
3. M. Moniruzzaman, K. I. Winey, *Macromolecules*, 2006, **39**, 5194.
4. E. D. Laird, C. Y. Li, *Macromolecules*, 2013, **46**, 2877.
5. Z. Spitalsky, D. Tasis, K. Papagelis, C. Galiotis, *Prog. Polym. Sci.*, 2010, **35**, 357.
6. A. Hirsch, *Angew. Chem. Int. Ed.*, 2002, **41**, 1853.
7. C.-Y. Hu, Y.-J. Xu, S.-W. Duo, R.-F. Zhang, M.-S. Li, *J. Chin. Chem. Soc.*, 2009, **56**, 234.
8. L. J. Meng, C. L. Fu, Q. H. Lu, *Prog. Nat. Sci.*, 2009, **19**, 801.
9. P. Singh, S. Campidelli, S. Giordani, D. Bonifazi, A. Bianco, M. Prato, *Chem. Soc. Rev.*, 2009, **38**, 2214.
10. Y.-L. Zhao, J. F. Stoddart, *Accounts Chem. Res.*, 2009, **42**, 1161.
11. J. N. Fowler, B. R. Chapman, D. L. Green, *Eur. Polym. J.*, 2010, **46**, 568.
12. S. Rana, J. W. Cho, *Nanoscale*, 2010, **2**, 2550.
13. G. Clave, S. Campidelli, *Chem. Sci.*, 2011, **2**, 1887.
14. V. N. Khabashesku, *Russ. Chem. Rev.*, 2011, **80**, 705.
15. C. Y. Li, L. Li, W. Cai, S. L. Kodjie, K. K. Tenneti, *Adv. Mater.*, 2005, **17**, 1198.
16. L. Y. Li, C. Y. Li, C. Y. Ni, *J. Am. Chem. Soc.*, 2006, **128**, 1692.
17. L. Y. Li, B. Li, M. A. Hood, C. Y. Li, *Polymer*, 2009, **50**, 953.
18. J. Z. Xu, T. Chen, C. L. Yang, Z. M. Li, Y. M. Mao, B. Q. Zeng, B. S. Hsiao, *Macromolecules*, 2010, **43**, 5000.
19. L. Y. Li, C. Y. Li, C. Y. Ni, L. X. Rong, B. Hsiao, *Polymer*, 2007, **48**, 3452.
20. J. H. Yang, C. Y. Wang, K. Wang, Q. Zhang, F. Chen, R. N. Du, Q. Fu, *Macromolecules*, 2009, **42**, 7016.
21. J. H. Yang, K. Wang, H. Deng, F. Chen, Q. Fu, *Polymer*, 2010, **51**, 774.
22. N. Y. Ning, W. Zhang, Y. S. Zhao, C. Y. Tang, M. B. Yang, Q. Fu, *Polymer*, 2012, **53**, 4553.
23. R. Haggenmueller, J. E. Fischer, K. I. Winey, *Macromolecules*, 2006, **39**, 2964.
24. L. Y. Li, Y. Yang, G. L. Yang, X. M. Chen, B. S. Hsiao, B. Chu, J. E. Spanier, C. Y. Li, *Nano Lett.*, 2006, **6**, 1007.
25. S. L. Kodjie, L. Y. Li, B. Li, W. W. Cai, C. Y. Li, M. Keating, *J. Macromol. Sci. B*, 2006, **45**, 231.
26. N. Y. Ning, F. Luo, B. F. Pan, Q. Zhang, K. Wang, Q. Fu, *Macromolecules*, 2007, **40**, 8533.
27. J. Yue, Q. Xu, Z. W. Zhang, Z. M. Chen, *Macromolecules*, 2007, **40**, 8821.
28. Z. W. Zhang, Q. Xu, Z. M. Chen, J. Yue, *Macromolecules*, 2008, **41**, 2868.
29. L. Zhang, T. Tao, C. Z. Li, *Polymer*, 2009, **50**, 3835.
30. S. J. Zhang, W. Lin, X. F. Yu, C. P. Wong, S. Z. D. Cheng, D. G. Bucknall, *Macromol. Chem. Phys.*, 2010, **211**, 1003.
31. S. J. Zhang, W. Lin, C. P. Wong, D. G. Bucknall, S. Kumar, *ACS Appl. Mater. Interfaces*, 2010, **2**, 1642.
32. L. Y. Li, W. D. Wang, E. D. Laird, C. Y. Li, M. Defaux, D. A. Ivanov, *Polymer*, 2011, **52**, 3633.
33. E. D. Laird, W. D. Wang, S. Cheng, B. Li, V. Presser, B. Dyatkin, Y. Gogotsi, C. Y. Li, *ACS Nano*, 2012, **6**, 1204.
34. W. D. Wang, C. Y. Li, *ACS Macro Lett.*, 2014, **3**, 175.
35. W. D. Wang, Z. Y. Huang, E. D. Laird, S. J. Wang, C. Y. Li, *Polymer*, 2015, **59**, 1.
36. G. Y. Zong, W. Zhang, N. Y. Ning, C. Y. Tang, M. B. Yang, Q. Fu, *Mol. Simulat.*, 2013, **39**, 1013.
37. L. Y. Li, B. Li, G. L. Yang, C. Y. Li, *Langmuir*, 2007, **23**, 8522.
38. G. Mago, D. M. Kalyon, F. T. Fisher, *J. Polym. Sci., Part B: Polym. Phys.*, 2011, **49**, 1311.
39. L. Chen, Z. H. Chen, X. Li, W. Huang, X. J. Li, X. K. Liu, *Polymer*, 2013, **54**, 1739.
40. M. Nie, D. M. Kalyon, F. T. Fisher, *ACS Appl. Mater. Interfaces*, 2014, **6**, 14886.
41. D. H. Zhang, M. A. Kandadai, J. Cech, S. Roth, S. A. Curran, *J. Phys. Chem. B*, 2006, **110**, 12910.
42. X. L. Zheng, Q. Xu, *J. Phys. Chem. B*, 2010, **114**, 9435.
43. N. Y. Ning, W. Zhang, Y. S. Zhao, F. Luo, Q. Fu, *Polym. Int.*, 2012, **61**, 1634.
44. N. Yu, L. H. He, Y. Y. Ren, Q. Xu, *Polymer*, 2011, **52**, 472.
45. F. Zhang, H. Zhang, Z. W. Zhang, Z. M. Chen, Q. Xu,

Macromolecules, 2008, **41**, 4519.
46. M. L. Minus, H. G. Chae, S. Kumar, *Macromol. Rapid Comm.*, 2010, **31**, 310.
47. M. C. García-Gutiérrez, J. J. Hernández, A. Nogales, P. Panine, D. R. Rueda, T. A. Ezquerra, *Macromolecules*, 2007, **41**, 844.
48. E. D. Laird, R. K. Bose, W. D. Wang, K. K. S. Lau, C. Y. Li, *Macromol. Rapid Comm.*, 2013, **34**, 251.
49. E. D. Laird, R. K. Bose, H. Qi, K. K. S. Lau, C. Y. Li, *ACS Appl. Mater. Interfaces*, 2013, **5**, 12089.
50. Y. Y. Zhang, K. N. Song, J. S. Meng, M. L. Minus, *ACS Appl. Mater. Interfaces*, 2013, **5**, 807.
51. J. H. Liu, J. H. Zou, L. Zhai, *Macromol. Rapid Comm.*, 2009, **30**, 1387.
52. B. Li, L. Li, B. Wang, C. Y. Li, *Nat. Nanotechnol.*, 2009, **4**, 358.
53. W. D. Wang, E. D. Laird, B. Li, L. Y. Li, C. Y. Li, *Sci. China Chem.*, 2012, **55**, 802.
54. W. R. Wang, X. M. Xie, X. Y. Ye, *Carbon*, 2010, **48**, 1680.
55. B. J. Jungnickel, *Lect. Notes Phys.*, 2003, **606**, 208.
56. J. P. Liu, B. J. Jungnickel, *J. Polym. Sci. Part B., Polym. Phys.*, 2007, **45**, 1917.
57. H. D. Keith, J. F. J. Padden, T. P. Russell, *Macromolecules*, 1989, **22**, 666.
58. H. L. Chen, H. H. Liu, J. S. Lin, *Macromolecules*, 2000, **33**, 4856.
59. W. T. Chuang, U. S. Jeng, H. S. Sheu, P. D. Hong, *Macromol. Res.*, 2006, **14**, 45.
60. W. T. Chuang, U. S. Jeng, P. D. Hong, H. S. Sheu, Y. H. Lai, K. S. Shih, *Polymer*, 2007, **48**, 2919.
61. J. M. Schultz, *Macromolecules*, 2012, **45**, 6299.
62. J. M. Schultz, *Front. Chem. China*, 2010, **5**, 262.
63. J. S. Qiu, C. Y. Xing, X. J. Cao, H. T. Wang, L. Wang, L. P. Zhao, Y. J. Li, *Macromolecules*, 2013, **46**, 5806.
64. J. S. Qiu, J. P. Guan, H. T. Wang, S. S. Zhu, X. J. Cao, Q. L. Ye, Y. J. Li, *J. Phys. Chem. B*, 2014, **118**, 7167.
65. L. J. Ye, X. C. Shi, C. C. Ye, Z. L. Chen, M. M. Zeng, J. C. You, Y. J. Li, *ACS Appl. Mater. Interfaces*, 2015, **7**, 6946.
66. J. P. Penning, R. St. John Manley, *Macromolecules*, 1996, **29**, 77.
67. K. Fujita, T. Kyu, R. St. John Manley, *Macromolecules*, 1996, **29**, 91.
68. L.-Z. Liu, B. Chu, J. P. Penning, R. S. J. Manley, *Macromolecules*, 1997, **30**, 4398.
69. I. Isayeva, T. Kyu, R. St. John Manley, *Polymer*, 1998, **39**, 4599.
70. E. Meaurio, N. Lo´pez-Rodrıguez, J. R. Sarasua, *Macromolecules*, 2006, **39**, 9291.
71. X. Hu, H. N. An, Z. M. Li, Y. Geng, L. B. Li, C. L. Yang, *Macromolecules*, 2009, **42**, 3215.
72. S. H. Mushrif, A. D. Rey, H. Tekinalp, *Ind. Eng. Chem. Res.*, 2008, **47**, 3883.

For Table of Content use only

Block-assembling: A New Strategy of Fabricating Conductive Nanoporous Materials from Nanocomposites Based on a Melt-miscible Crystalline/Crystalline Blend and MWCNTs

*Lijun Ye, Cuicui Ye, Xianchun Shi, Hongyan Zhao, Kangyuan Xie, Depei Chen, Yongjin Li**

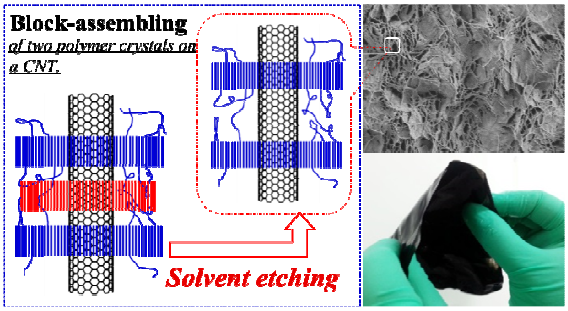

A "block-assembling" strategy is explored to fabricate conductive nanoporous polymeric materials with unique interposition structure of CNTs in the inner wall of the internal pores.